PCCP

Accepted Manuscript

ROYAL SOCIETY OF CHEMISTRY

www.rsc.org/pccp

Ordered Carbon Nanotubes/n-Dodecyl Tetraethylene Monoether Liquid Crystal Composites through Phase Separation Induced by Poly (ethylene glycol)

Lin Wang [a], Xia Xin [a, b *], Kai Guo [a], Mengzhou Yang [a], Xin Ma [a], Jing Yuan [a], Jinglin Shen [a], Shiling Yuan [a *]

[a] *Key Laboratory of Colloid and Interface Chemistry (Shandong University), Ministry of Education, Shanda nanlu No. 27, Jinan, 250100, P. R. China*

[b] *National Engineering Technology Research Center for Colloidal Materials, Shandong University, Shanda nanlu No. 27, Jinan, 250100, P. R. China*

[*] Author to whom correspondence should be addressed, E-mail: xinx@sdu.edu.cn.

Phone: +86-531-88363597. Fax: +86-531-88361008

[*] Author to whom correspondence should be addressed, E-mail: shilingyuan@sdu.edu.cn.

Phone: +86-531-88365896. Fax: +86-531-88564750

Abstract

Carbon nanotubes (CNTs) were incorporated into a lyotropic liquid crystal (LLC) matrix at room temperature through spontaneous phase separation. The phase separation process was occurred in n-dodecyl tetraethylene monoether ($C_{12}E_4$) solutions induced by hydrophilic polymer, poly (ethylene glycol) (PEG). It was found the molecular weight of PEG has significant effect on CNTs/$C_{12}E_4$ system which not only influences the phase behavior of the system but also changes the properties of the CNTs-LLC composite. Polarized optical microscopy (POM) images, combined with small-angle X-ray scattering (SAXS) results, indicate that CNTs incorporated in the layers of the lamellar LLCs without destroying the structure of LLCs. Moreover, UV-vis absorption, Raman spectra and rheological measurements were performed to investigate the characteristic properties of CNTs-LLC composites. This study not only gives a more comprehensive understanding on the polymer-induced phase separation, but also expands potential uses of CNTs/LLC composites in nanotechnology.

Introduction

Given their high aspect ratio, extraordinary mechanical properties and ultra-high electrical conductivity, carbon nanotubes (CNTs) have attracted a lot of attention due to their wide applications in many aspects ranging from optoelectronics to biomedicine [1-3]. Commonly, for the consideration of perfectly representing their utility, the CNTs have to be well dispersed and even orderly oriented in appropriate matrix. However, as the CNTs are solvophobic and prone to aggregate through van der Waals interactions in almost all kinds of matrix [4], they usually form commonly-known "spaghetti-like" bundles in which each tubular framework is randomly oriented, thus showing limited hierarchical organization and poor property performance. Therefore, great efforts including covalent and noncovalent methods have been made to disperse CNTs into proper medium in recent years. Among them, the noncovalent method, typically with the help of surfactants [5, 6], polymers [7, 8], and natural biomolecules [9, 10], has been considered to be effective and convenient.

Although great progress has been made in the field of CNT dispersion, the CNTs are usually randomly oriented in the dispersions. As CNTs are anisotropic nanoparticles with an extreme aspect ratio, they exhibit most of their remarkable properties along the tube axis [11]. The uniform alignment of CNTs is therefore a crucial condition for most of the fascinating applications proposed to CNTs. A great deal of research has been devoted to developing procedures for aligning dispersed nanotubes and methods including shearing, magnetic- or electric-field application, and 'molecular combing' [12-15]. But in order to obtain samples where CNTs are both well dispersed and oriented, some researchers also have focused their attention on nanotube alignment by using liquid-crystal (LC) phases [16-30]. LC with their fluidity but at the same time with their long range organization

represents an interesting novel route for realizing functional composites. In the ordered phase the molecules tended to align along a common direction forming orientationally ordered macroscopic domains [31], hence LC can provide a way to control the orientation of the nanotubes [32].

Since the viscosity of LLC is usually high at room temperature, a heating process is normally applied which may destroy the CNTs/LLC composites due to desorption of the nonionic surfactant at high temperature [33]. Recently, we have shown that the heating process can be avoided and CNTs/LLC composites can be fabricated at room temperature via phase separation of non-ionic surfactant in the presence of a nonionic polymer such as poly (ethylene glycol) (PEG) [33-35]. In the present work, we report a detailed study on incorporation of CNTs into n-dodecyl tetraethylene monoether ($C_{12}E_4$) LLC by phase separation using different molecular weights of PEG. The performance of CNTs/ $C_{12}E_4$ LLC composites were characterized by visual inspection, UV-vis-NIR, polarized microscopy observations (POM), small-angle X-ray scattering (SAXS), Raman spectra, and rheological measurements. The results indicated that by applying a $C_{12}E_4$/PEG phase separation method, CNTs can be efficiently incorporated to the upper LLC phase and the molecular weight of PEG had significant effects on the phase separation method. Our experimental results may open the avenue of new applications for surfactant/polymer phase separation process.

Experimental Section

Chemicals and Materials.

SWNTs, with a diameter of < 2 nm and a length of 2-15 μm, were purchased from Shenzhen Nanotech Port Co., Ltd., which were prepared by chemical vapor deposition (CVD). The remaining is mainly catalyst and amorphous carbon. $C_{12}E_4$ was purchased from Acros Organics (USA) with a purity better than 99%. PEG with different molecular weight (800, 1000, 2000, 4000, 6000, 10000,

12000 and 20000 g mol^{-1}) were purchased from Sinopharm Chemical Reagent Company. All the above reagents were used without further purification. Water used in the experiments was triply distilled by a quartz water purification system.

Preparation of CNTs/ $C_{12}E_4$ LLC Composites.

The phase separation method used to incorporate CNTs into LLC matrix can be schematically shown in Scheme 1. First, stock solution of 0.1 wt % $C_{12}E_4$ was prepared by dissolving the desired amount of $C_{12}E_4$ in water at room temperature. Dispersions of CNTs in 0.1 wt % $C_{12}E_4$ aqueous solution were obtained by sonicating the mixtures at 40 kHz and 250 W using KQ-250DB ultrasonic apparatus (Shanghai). After 45 min, a homogeneous black dispersion was obtained (Scheme 1A). The as-prepared CNTs dispersions contain well-dispersed CNTs as well as tube bundles. Small amount of black precipitates were noticed after deposition at room temperature for 2 weeks. The upper phase, which can be stable at room temperature for months, was collected for further use.

Desired amounts of PEG and $C_{12}E_4$ were added to aqueous dispersions of CNTs in 0.1 wt % $C_{12}E_4$ to make sure the weight percent of $C_{12}E_4$: PEG: dispersions of CNTs/$C_{12}E_4$ = 1: 2: 7. The mixtures were homogenized by stirring for about 10 minutes (Scheme 1B). Then the mixture was allowed to equilibrate at room temperature, during which simultaneous phase separation was noticed. Finally two phases were formed: an upper CNTs/$C_{12}E_4$ LLC Composites and a bottom transparent isotropic phase (Scheme 1C). According to the ratio of the upper liquid crystal phase to the whole sample volume, it is calculated that the concentration of CNTs in the upper phase is in the range of 0.04 ~ 0.1 wt %.

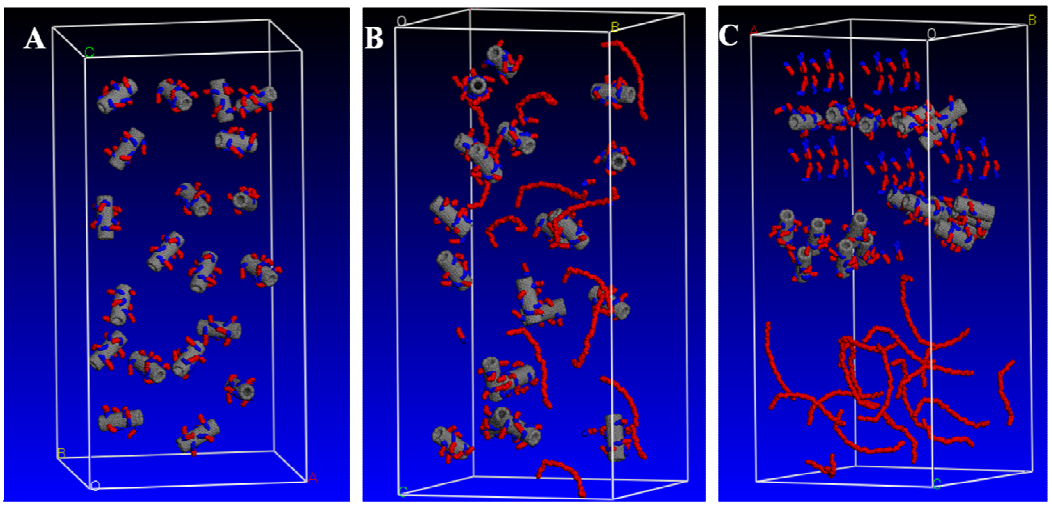

: CNTs; : $C_{12}E_4$; : PEG.

Scheme 1 Schematic illustration of the phase separation process: (A) CNTs dispersion in 0.1 wt % $C_{12}E_4$ aqueous solution; (B) mixture of CNTs dispersion, $C_{12}E_4$ and PEG after being homogenized; (C) final state after equilibrium of phase separation.

Methods and Characterization

UV-vis-NIR measurements were carried out on a computer-manipulated spectrometer (UV-vis 4100, Hitashi, Japan). HRTEM observations was carried out on a JEOL JEM-2100 microscope (Japan) at an accelerating voltage of 200 kV. Samples were prepared by directly dipping a ultrathin carbon-coated copper grid into the sample, which were then dried by using an NIR lamp before observation. Polarized optical microscopy observations were performed by an AXIOSKOP 40/40 FL (ZEISS, Germany) microscope. Samples were prepared by dropping several drops of solution into a 1 mm thick trough, which was covered by another glass slide to avoid solvent evaporation.

The obtained LC phases were characterized by an HMBG-SAX X-ray small-angle scattering system (Austria) with a Ni-filtered Cu Kα radiation (0.154 nm) operating at 50 kV and 40 mA. The distance between the sample and detector was 27.8 cm. Raman spectra were obtained from an NXR

FT-Raman module (Nexus 670, Nicolet Co.) equipped with a Ge detector. The samples were excitated by a laser source with a wavelength of 1064 nm and a power of 0.103 W.

The rheological measurements were carried out on a HAAKE RS75 rheometer with a cone-plate system (Ti, diameter, 35 mm; cone angle, 1°). For the shear-dependent behavior, the viscosity measurements were carried out at shear rates ranging from 0 to 1000 s^{-1}. In oscillatory measurements, an amplitude sweep at a fixed frequency of 1 Hz was performed prior to the following frequency sweep in order to ensure that the selected stress was in the linear viscoelastic region. The viscoelastic properties of the samples were determined by oscillatory measurements in the frequency range of 0.01-10 Hz. The samples were measured at 20.0 ± 0.1 °C with the help of a cyclic water bath.

Results and discussion

Dispersion State of CNTs in 0.1 wt % $C_{12}E_4$ Aqueous Solution.

A series of samples with 10 mL 0.1 wt % $C_{12}E_4$ and increasing amount of CNTs are shown in Figure 1 and the effect of the amount of added CNTs on CNT/$C_{12}E_4$ dispersions was investigated. It can be seen that with increasing amount of added CNTs, the black color of the dispersions strengthens (Figure 1B). When the amount of added CNTs reaches 0.05 wt %, the color of the solutions becomes the darkest (Figure 1D) and then eventually become clear and colorless (Figure 1F). HRTEM image shown in Figure 1H demonstrates that the tubes tend to exist as individuals or very small bundles. This phenomenon was in sharp contrast to the case of raw materials which tend to aggregate into large ropes.

UV-vis-NIR measurements were carried out on these dispersions (Figure 2A) and the inset of

Figure 2A is a magnified curve for curve f in the 650 -900 nm region. The spectroscopic features of CNTs depend only on their diameter and helicity [36]. Typically, dispersed SWNTs have three sections of absorptions in the UV-vis-NIR region: the first van Hove transitions, E11, of the direct band gap semiconducting tubes located at 800-1600 nm, slightly overlapping the 550-900 nm region of their E22 transitions and the lowest energy van Hove transitions of the metallic tubes located around 400-600 nm. In practice, however, one could only get the average spectroscopic characteristics of dispersed nanotubes because the SWNTs used are always a mixture which is polydisperse both in tube diameter and helicity [37, 38]. Moreover, it was also found that the absorbance intensity did not increase continuously with increasing amount of CNTs. Instead, it passed through a maximum at 0.05 wt % and then decreased (Figure 2B). This conclusion is consistent with the sample observations.

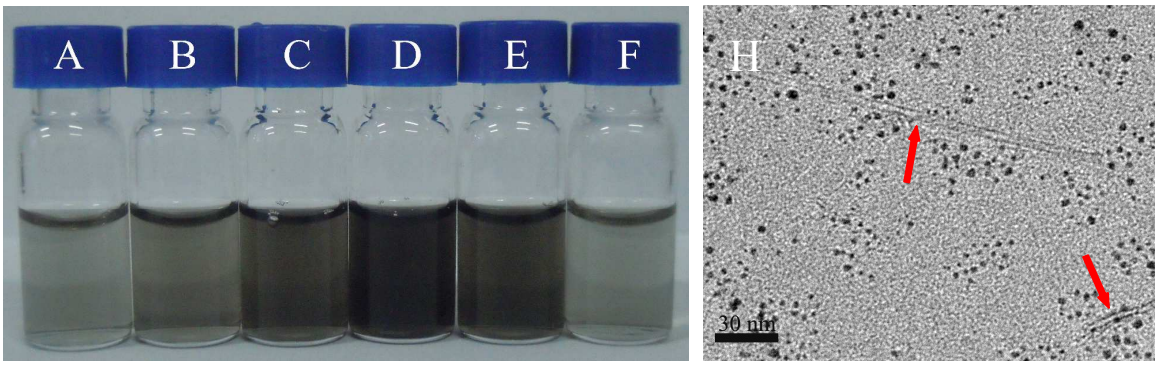

Figure 1 Dispersions of CNTs in 10 mL of 0.1wt % $C_{12}E_4$ aqueous solutions with increasing amount of added CNTs: (A) 0.01 wt %, (B) 0.02 wt %, (C) 0.04 wt %, (D) 0.05 wt %, (E) 0.08 wt %, (F) 0.1 wt %. The images were taken more than two weeks after preparation. (H) HRTEM images of 0.02 wt % CNTs dispersed in 10 mL of 0.1 wt % $C_{12}E_4$ aqueous solution.

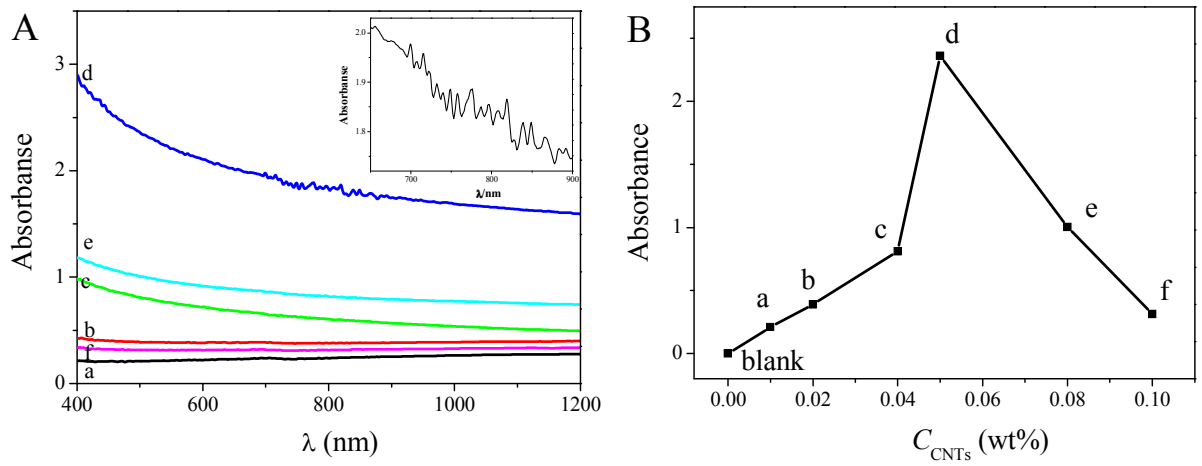

Figure 2 UV-vis-NIR absorptions in the (A) 400-1200 nm and (B) Absorbance intensity for the dispersions of CNTs dispersed in 10 mL of 0.1wt % $C_{12}E_4$ (λ = 800 nm). Curves a-f corresponded to samples A-F in Figure 1. The inset of (A) is a magnified curve for curve d in the 650 -900 nm region.

Phase behavior of $C_{12}E_4$-PEG-H_2O system

In order to study the influence of the molecular weight of PEG on $C_{12}E_4$ solution, a simple study on the phase behavior of the ternary $C_{12}E_4$-PEG-H_2O system was performed and the result is shown in Figure 3. It can be seen that when the molecular weight of PEG is below 1000 g mol^{-1}, no phase separation was observed (Figure 3 A, B). Sample B is ivory-white and more cloudy than sample A. When the molecular weight of PEG exceeds 2000 g mol^{-1} (Figure 3C-H), phase separation occurs with a bottom transparent isotropic phase and an upper viscous phase. Moreover, the upper phase was later confirmed to be lamellar liquid crystals by the typical maltese crosses texture under POM (Figure 4A-C).

The physical origin of the phase behavior observed above is related to entropic interactions leading to osmotic depletion forces [39]. Several studies of depletion-induced phase separations were

reported in colloidal systems [40, 41]. In the case of micellar/polymer solutions, it was demonstrated that the lamellar ordering of surfactants was induced only when the polymer radius of gyration, R_G, was larger than the size of the water channels, L_{water}, in the lamellar phase [42]. In the present study, the radius of gyration for PEG calculated according to the equation $R_G = 0.02M^{0.58}$ nm are 1.0 nm (PEG 800), 1.1 nm (PEG 1000), 1.6 nm (PEG 2000), 2.5 nm (PEG 4000), 3.1 nm (PEG 6000), 4.2 nm (PEG 10000), 4.6 nm (PEG 12000), 6.2 nm (PEG 20000), respectively [43]. The size of the water channel (L_{water}) between the layers of the lamellar phase for $C_{12}E_4$ is 1.6 nm. It means the radius of gyration for PEG with molecular weight higher than 2000 are larger than the water channel in the lamellar phase of $C_{12}E_4$ (depletion interactions), so the phase separation occurred and ordered $C_{12}E_4$-rich phase was formed.

Figure 3 Photographs of the phase behavior of $C_{12}E_4$ solution in the presence of different molecular weight of PEG. The molecular weights of PEG are (A) 800, (B) 1000, (C) 2000, (D) 4000, (E) 6000, (F) 10000, (G) 12000, (H) 20000 g mol^{-1}, respectively. The weight fractions of $C_{12}E_4$ and PEG to water before phase separation were 10 wt % and 20 wt %, respectively.

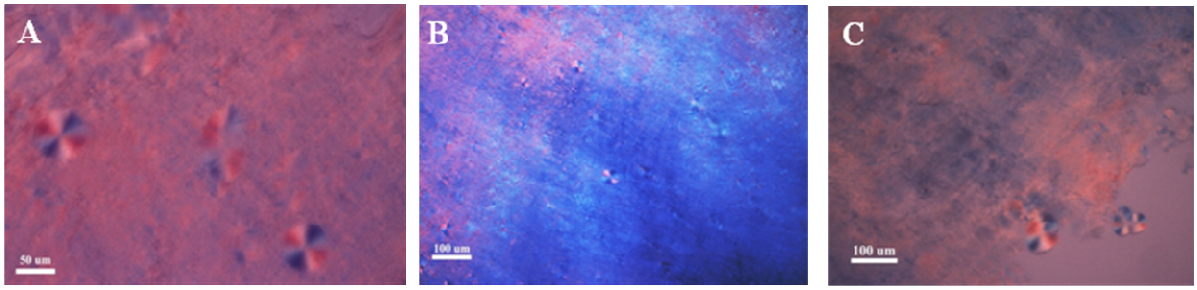

Figure 4 POM images for $C_{12}E_4$ liquid crystal phases formed by phase separation in the presence of different molecular weight of PEG: (A) 2000; (B) 12000; (C) 20000 g mol^{-1}.

Influence of molecular weight of PEG on CNTs/LLC composites

When CNTs were incorporated into the upper LLC phase by phase separation in the presence of PEG, it can be seen that the textures of the LLC phase change from typical maltese crosses texture [44] to parallel-banded structures (Figure 5A-C). We speculate that this is due to the ordering of the CNTs which induced the refraction of light with a fixed direction. From these results, the alignment of CNTs in the LLC phase can be deduced.

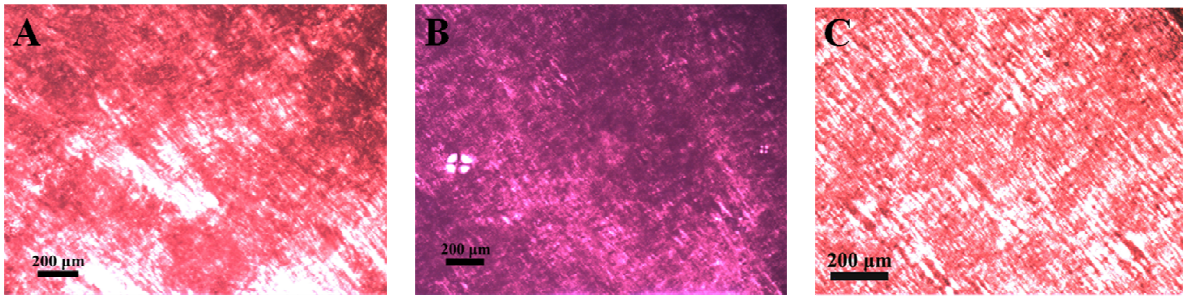

Figure 5 POM images for CNTs/$C_{12}E_4$ liquid crystal phases formed by phase separation in the presence of different molecular weight of PEG: (A) 2000; (B) 12000; (C) 20000 g mol^{-1}. The weight fractions of $C_{12}E_4$ and PEG to water before phase separation are 10 wt % and 20 wt %, respectively and CNTs in 0.1 wt % $C_{12}E_4$ dispersion was fixed at 0.02 wt %.

Rheological measurements can give macro properties of the system in real-time, then reflect the change of internal microstructure and provide more details about difference of the system [45]. The amplitude sweep (f =1 Hz) in Figure 6A indicates the weak dependence of G′ (105.3 Pa) and G″ (21.3 Pa) on applied stress until the yield stress (≈ 4.8 Pa) is reached when the molecular weight of PEG is 2000. When the molecular weight of PEG is increased, the LLC mechanical intensity can be greatly enhanced. For example, the G′ and G″ increase to 551.7 and 94.5 Pa, respectively, as the

molecular weight of PEG increases to 20000. Meanwhile, the yield stress is also improved to 25.8 Pa. Moreover, the complex viscosity (η^*) decreases with the increase of frequency for these three samples (Figure 6B). For $C_{12}E_4$ LLC induced by PEG 2000, at low frequencies, G″ is larger than G′, showing a viscous behavior. At higher frequencies, however, G′ is larger than G″, exhibiting an elastic behavior (Figure 6C). But for $C_{12}E_4$ LLC induced by PEG 12000 and PEG 20000, G′ is higher than G″ over the investigated oscillating frequency and exhibits typical gel-like behavior. Furthermore, it is noticeable that G′, G″ and η^* increase with the increase of the molecular weight of PEG, indicating the more condensed LLC induced by higher molecular weight of PEG.

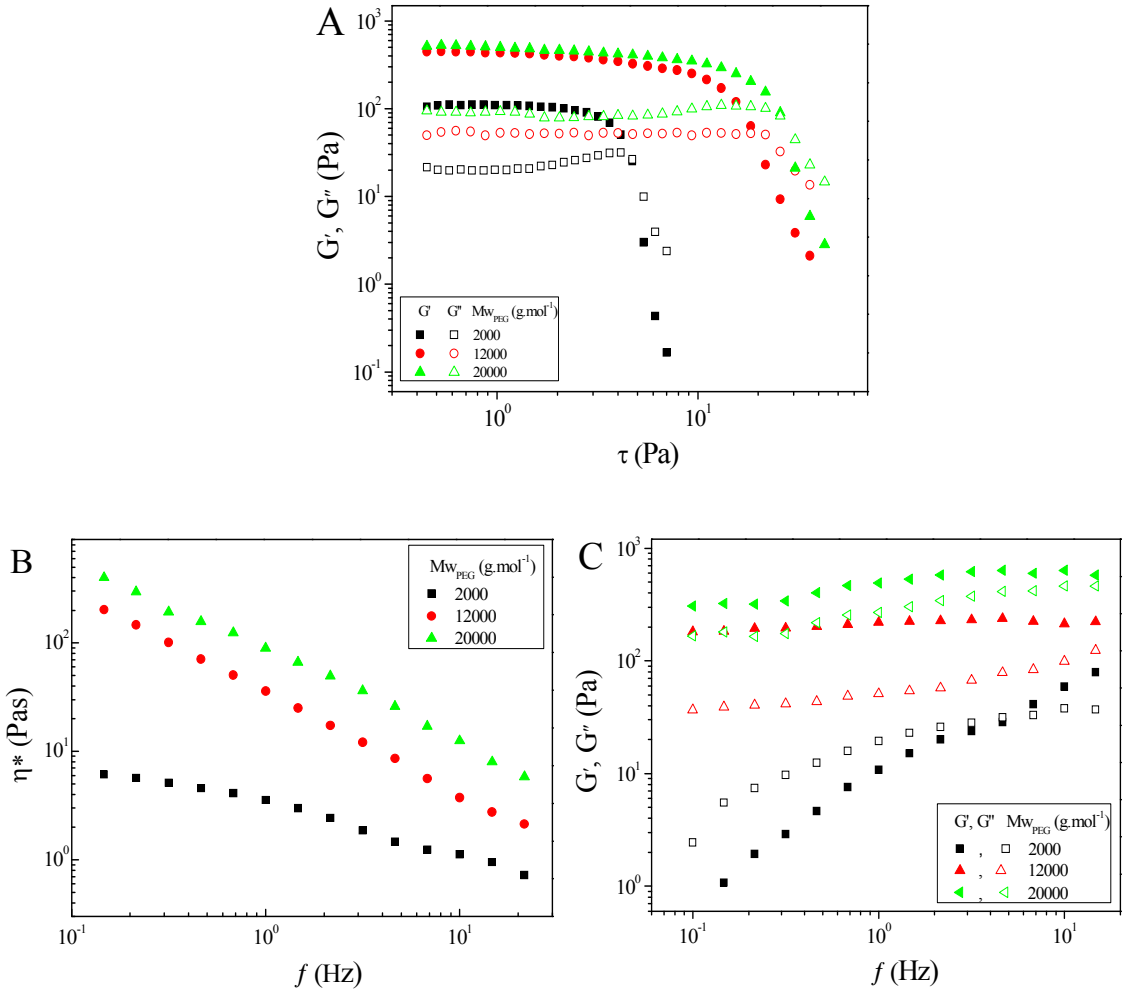

Figure 6 Rheological results for CNTs/LLC composites with increasing PEG molecular weight. (A)

Elastic modulus (G′) and viscous modulus (G″) as a function of the applied stress at a constant frequency (1.0 Hz); Variation of (B) complex viscosity and (C) G′ and G″ as a function of frequency. The weight fractions of $C_{12}E_4$ and PEG to water before phase separation were 10 wt % and 20 wt %, respectively and CNTs in 0.1 wt % $C_{12}E_4$ dispersion was fixed at 0.02 wt %, respectively.

To gain further details about CNTs/LLC composites, SAXS measurements were carried out to characterize properties of the ordered surfactant phase as a function of molecular weight of PEG (Figure 7). Two peaks were detected with a relative position ratio of 1:2, as expected for the (100) and (110) reflections of the lamellar phase. Interestingly, with increasing molecular weight of PEG, the d-spacing of the lamellar lattice, calculated from the q value of the first peak ($d = 2\pi/q_{max}$), decreased continuously. For example, the d-spacing of the lamellar phase in the presence of PEG 4000 is 5.56 nm. It shifts to 5.37 nm when the molecular weight of PEG changes to 20000 g mol^{-1}. This observation clearly indicates that the increase of molecular weight of PEG does cause some changes of the host lamellar matrix and make it more concentrated, which is also consistent with rheological results.

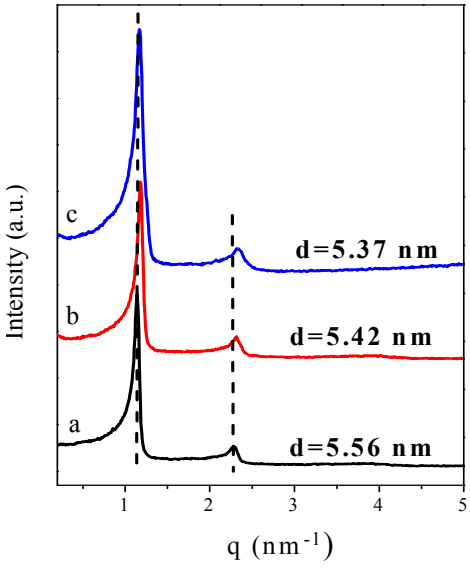

Figure 7 SAXS results of CNTs/LLC composites in the presence of different molecular weight of PEG: (a) 2000; (b) 12000; (c) 20000 g mol^{-1}. The weight fractions of $C_{12}E_4$ and PEG to water before

phase separation are 10 wt % and 20 wt %, respectively and CNTs in 0.1 wt % $C_{12}E_4$ dispersion was fixed at 0.02 wt %. Two dashed lines are guides to the eyes.

Influence of the concentration of CNTs on CNTs/LLC composites

The concentration of CNTs has significant effects on the properties of CNTs/LLC composites. Figure 8 shows CNTs/LLC composite with different CNTs content obtained after phase separation. It was found that as the concentration of CNTs increases, the color of the CNTs/LLC composites also becomes heavier (Figure 8A-D).

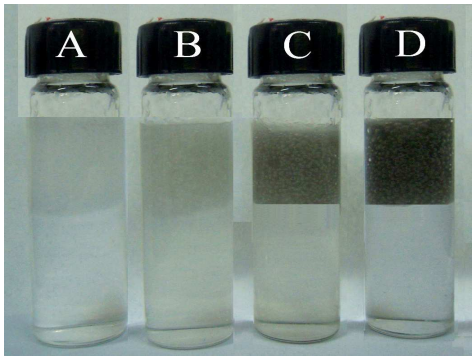

Figure 8 CNTs embedded in the upper LLC phase formed by $C_{12}E_4$ (10 wt %) after phase separation induced by PEG 20000 (20 wt %). The weight percent of SWNTs in the upper phase was calculated to be (A) 0 wt %, (B) 0.04 wt %, (C) 0.08 wt % and (D) 0.1 wt % which enhanced two times compared with the dispersion of SWNTs in 0.1 wt % $C_{12}E_4$.

It can be seen from Figure 9 that as the shear rate is increased, the viscosity is decreased with increasing the shear rate, indicating the shear-thinning behavior of the system. In addition, it also can be seen that the viscosity of the system increased firstly and then decreased with the increase of the concentration of CNTs. In the whole frequency measurement, the system showed a strong elastic response. The η^* decreases and G′ and G″ increased with the increase of frequency and G′ is higher than G″ over the whole frequency range. With the increase of the concentration of CNTs, the viscoelastic properties of the system also increased firstly and then decreased.

It is well-known that CNTs are considered to be a reinforcing agent of mechanical properties of

nanocomposites. However, in our study, it was found that adding a small amount of CNTs can enhancement the strength of the CNTs/LLC composite and with the increase of the concentration of CNTs the intensity increased gradually. But adding excessive concentration of CNTs induces the decrease of the strength of CNTs/LLC composite. The states of CNTs/LLC composites as a function of the concentration of incorporated CNTs in the upper LLC phase are shown in Scheme 2. We conjecture that it can create efficient steric repulsions between individual CNTs and enhance the strength of the system with the addition of a small amount of CNTs and reached a maximum at a suitable concentration. When the concentration of CNTs is excessive, the steric effect of $C_{12}E_4$ is insufficient to make the CNTs independent of each other. This causes flocculation and twine of dispersed CNTs, thereby destroy the long-range ordering of liquid crystal and ultimately decline in strength of CNTs/LLC composite.

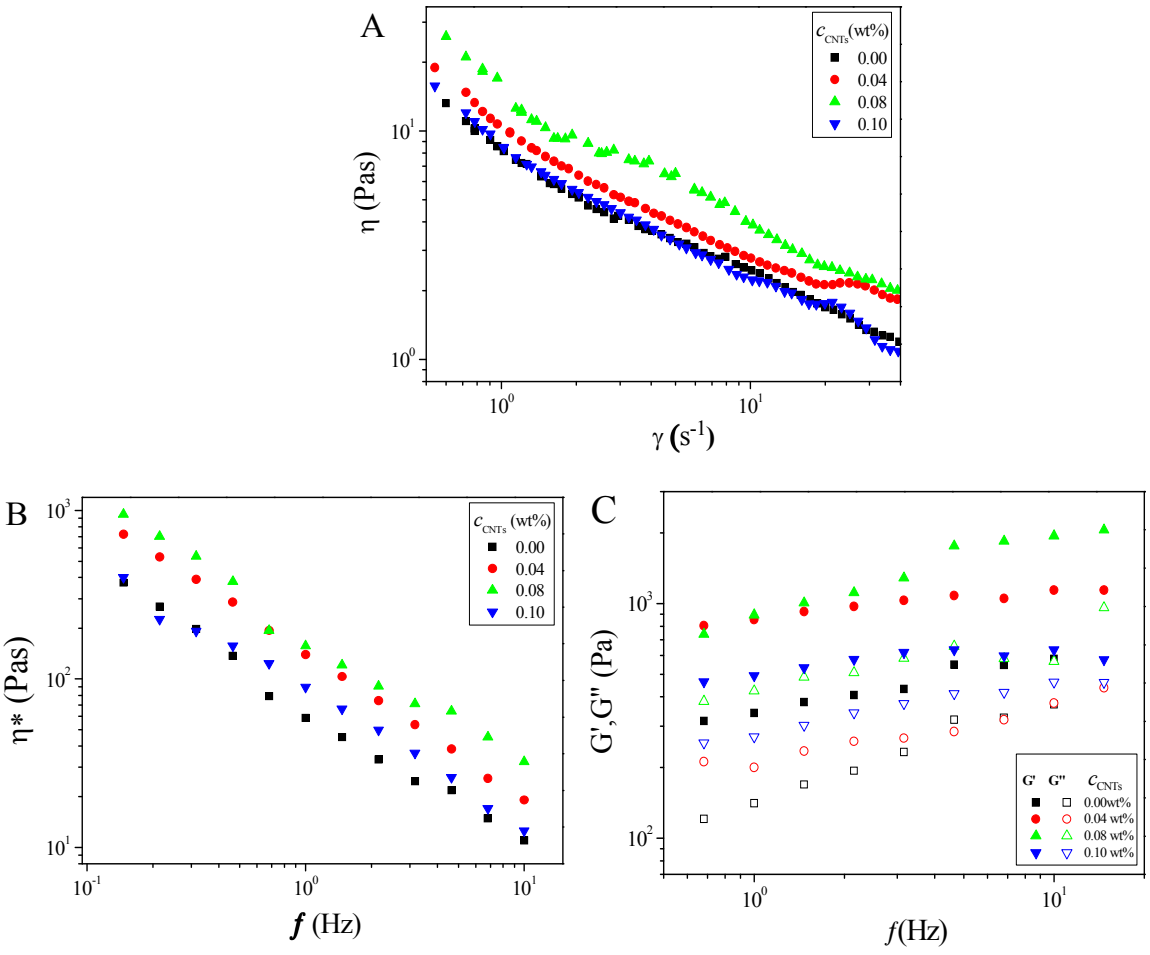

Figure 9 Rheological results for CNTs/LLC composites with increasing the concentration of CNTs. (A) Variation of shear viscosity as a function of shear rate, (B) G′ and G″ as a function of the applied stress at a constant frequency (1.0 Hz), (C) Variation of G′ and G″ as a function of frequency. The weight fractions of $C_{12}E_4$ and PEG 20000 to water before phase separation were 10 wt % and 20 wt %, respectively.

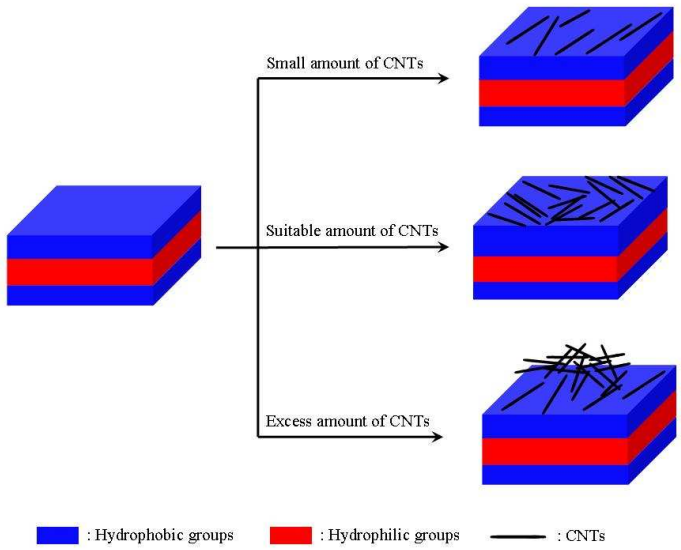

Scheme 2 Schematic illustrations of the states of CNTs/LLC composites as a function of the concentration of incorporated CNTs in the upper LLC phase.

Figure 10 summarizes the SAXS results of CNTs/LLC composites (Figure 10A) and the changes of the d-spacing of the LLC matrix induced by different concentration of CNTs incorporation (Figure 10B). It can be seen that the incorporation of CNTs first caused a continuous increase of the d-spacing of the host LLC matrix (from 5.15 nm to 5.51 nm). However, when the content of the incorporated CNTs reached 0.10 wt %, a decrease in d-spacing was noticed (from 5.51 nm to 5.42 nm). It was probably due to the microscopic phase separation of CNTs within the LLC matrix and these results are also consistent with rheological results above.

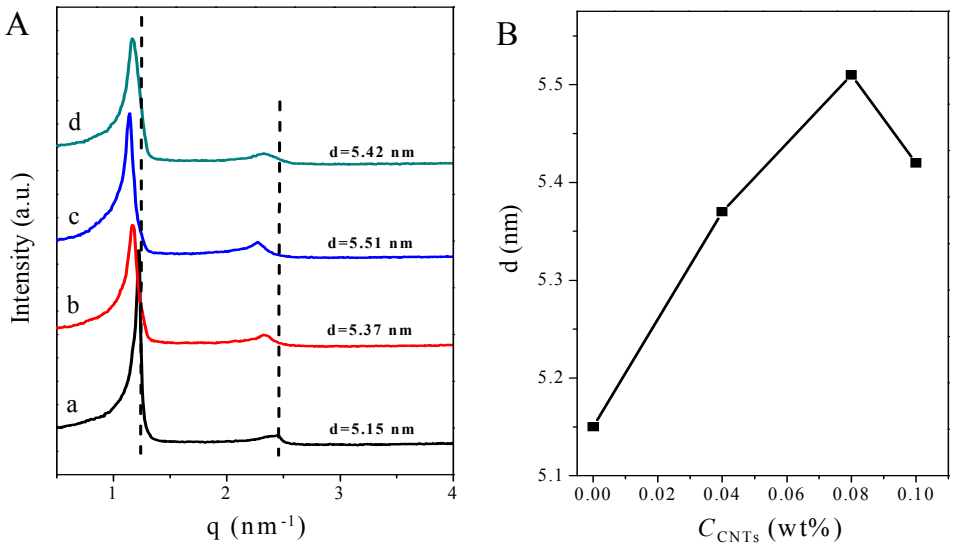

Figure 10 (A) SAXS results of CNTs/LLC composites as a function of the concentration of incorporated CNTs in the upper LLC phase: (a) 0, (b) 0.04 wt %, (c) 0.08 wt %, (d) 0.10 wt %. The weight fractions of $C_{12}E_4$ and PEG to water before phase separation are 10 wt % and 20 wt %, respectively. Two dashed lines are guides to the eyes. (B) The variation of d-spacing of the lamellar phases a function of the concentration of incorporated CNTs in the upper LLC phase.

Influence of concentration of PEG on CNTs/LLC composites

The influence of the concentrations of PEG on CNTs/LLC composites was also investigated. When the concentration of PEG 20000 is 4 wt %, the amplitude sweep (f =1 Hz) in Figure 11A indicates the weak dependence of G′ (226.7 Pa) and G″ (26.8 Pa) on applied stress until the yield stress (≈10 Pa) is reached. When the PEG 20000 concentration is increased, the LLC mechanical intensity can be greatly enhanced. For example, the G′ and G″ increase to 1144 and 147 Pa, respectively, as the concentration of PEG 20000 increases to 20 wt %. Meanwhile, the yield stress of this system is also improved to 115 Pa. In the whole frequency measurement, the system showed a strong elastic response. The η* decreases and the G′ and G″ increased with the increase of

frequency and G′ is higher than G″ over the whole frequency range. Moreover, both G′ and G″ increase with the increase of the concentration of PEG 20000 and accompanied with the higher viscosity, which also reflects the more condensed LLC phase.

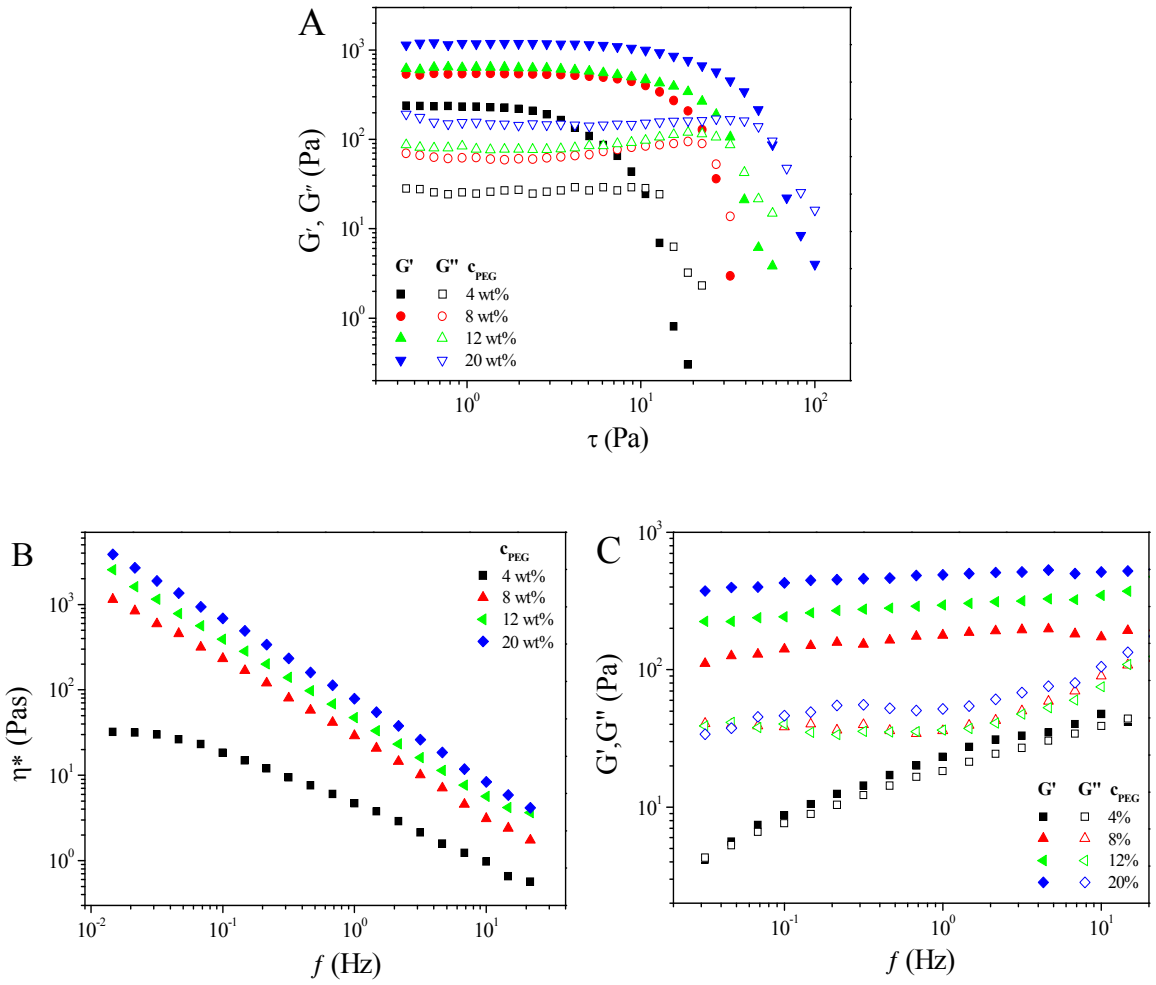

Figure 11 Rheological results for CNTs/LLC composites formed by phase separation in the presence of different concentration of PEG 20000. (A) G′ and G″ as a function of the applied stress at a constant frequency (1.0 Hz), (B) Variation of η* and (C) G′ and G″ as a function of frequency. The weight fraction of $C_{12}E_4$ to water before phase separation is 10 wt % and CNTs in 0.1 wt % $C_{12}E_4$ dispersion was fixed at 0.02 wt %.

When the amount of added PEG 20000 changed from 4 wt % to 20 wt % while the

concentration of $C_{12}E_4$ and CNTs were fixed at 10 wt % and 0.02 wt %, respectively, the upper LLC phases were always lamellar phase (Figure 12A); however, the higher concentration of PEG 20000 can capture more water molecules in the bottom phase which makes an decrease in d-spacing for the upper LLC phase (Figure 12B). Thus, it can be concluded that the upper LLC phase was more condensed at higher amount of added PEG 20000 and the concentration of CNTs in the upper LLC phase was also increased.

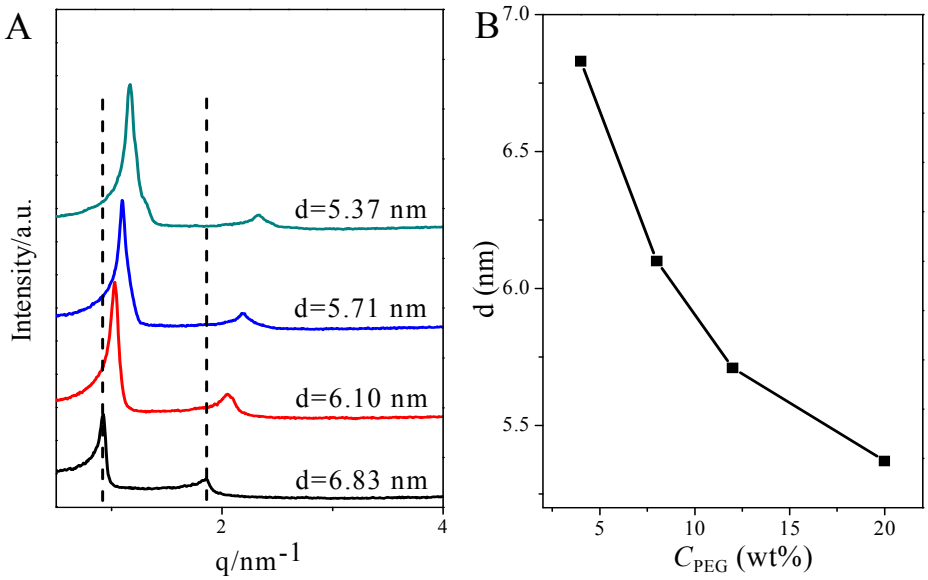

Figure 12 (A) SAXS results of CNTs/LLC composites as a function of the concentration of PEG 20000: (a) 4, (b) 8, (c) 12, (d) 20 wt %. The weight fractions of $C_{12}E_4$ to water before phase separation is 10 wt % and CNTs in 0.1 wt % $C_{12}E_4$ dispersion was fixed at 0.02 wt %. Two dashed lines are guides to the eyes. (B) The variation of d-spacing of the lamellar phases as a function of the concentration of PEG 20000.

Raman Spectra

Raman spectroscopy can provide important data for the understanding of the structure of CNTs and their physical properties and it is one of the powerful tools for the study of CNTs [46]. From

Raman spectroscopy, we can estimate vibration modulus of SWNTs and calibrate the diameter distribution of SWNTs and then get the structure characteristics, orientation effect, elastic modulus and other information of CNTs. As can be seen in Figure 13, the tangential G-peak and G*-peak of the raw CNTs were located around 1587 and 2540 cm^{-1}, respectively. The D-peak, which was usually caused by defects in the CNTs [47], was nearly negligible, indicating defects of the raw CNTs were rare (Figure 13b).

After dispersion into the bulk aqueous solution of $C_{12}E_4$, the position of the G-peak remained unchanged (Figure 13c), but the G*-peak nearly disappeared and the curve tends to protrude out of the baseline around 500 cm^{-1} probably due to the resonance effect between dispersed CNTs and adsorbed $C_{12}E_4$ molecules. After the CNTs incorporated to the upper $C_{12}E_4$ LLC phase, the curve returns to the location of the baseline (Figure 13 d) and in the right hand of D* at about 2878 cm^{-1}, there emerges a new peak. We hypothesized that G may be split into two peaks, one is a transverse mode (G-) and the other is a longitudinal mode (G+). If the carbon nanotube is composed of curled graphene, then the mode vibration along the diameter is G- and the mode vibration along the tube length is G+. This phenomenon is probably because of the alignment of CNTs in the liquid crystal which makes the different properties along diameter and length of CNTs. Thus, this is a good proof to reveal that the alignment of CNTs in the liquid crystal. It is also seen that the intensity of the D-peak of the dispersed CNTs is higher than that of the raw CNTs, indicating that the sonication conditions in our experiments cause a little destructions on the nanotubes (Figure 13c, d).

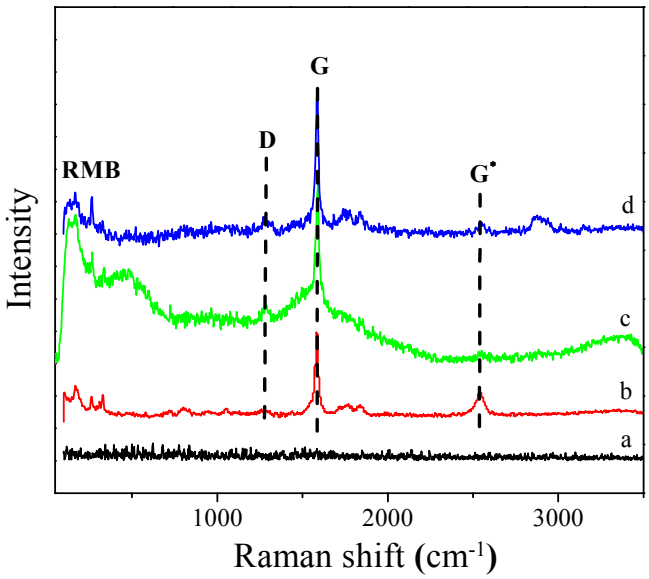

Figure 13 Raman spectra excitated at 1064 nm of (a) pure $C_{12}E_4$ LLC, (b) the raw CNTs, (c) 0.05 wt% CNTs dispersed in 10 mL of 0.1wt % $C_{12}E_4$ and (d) $C_{12}E_4$ LLC/CNTs composite.

Conclusion

To conclude, integration of CNTs into $C_{12}E_4$ lamellar LLC formed by phase separation in the presence of PEG with different molecular weights is demonstrated. CNTs-LLC composites preserved the parallel-banded structures of lamellar LLCs by POM observations. SAXS results indicate that the CNTs integrated within the layer of lamellar LLCs. The increase of d spacing indicates that the LLCs formed in $C_{12}E_4$ LLCs can impose a certain degree of alignment on the CNTs. The UV-vis and Raman spectra results further confirm that the CNTs have been incorporated in the LLC phase. The rheological results indicate that CNTs-LLC composites are highly viscoelastic due to the introduction of the CNTs. Moreover, different molecular weights of PEG show significant effects on the change of the properties of the systems of CNTs/$C_{12}E_4$. The future for LC-nanotube composites thus seems bright, with breakthroughs in carbon nanotube–LLC composites and it is confident that the research on this topic will produce more exciting results over

the next few years.

Acknowledgement

We gratefully acknowledge financial support from the Natural Science Foundation of China (21173128, 21203109) and Independent Innovation Foundation of Shandong University (IIFSDU, 2012GN015).

Notes and references

1 Z. Liu, W. Cai, L. He, N. Nakayama, K. Chen, X. Sun, X. Chen, H. Dai, *Nat. Nanotechnol*., 2007, **2,** 47–52.

2 N. Karousis, N. Tagmatarchis, D. Tasis, *Chem Rev*., 2010, **110,** 5366–5397.

3 K. S. Suman, A. Pal, S. Bhattacharya, C. N. R. Rao, *J. Mater. Chem*., 2010, **20,** 6881–6890.

4 P. Singh, S. Campidelli, S. Giordani, D. Bonifazi, A. Bianco, M. Prato, *Chem. Soc. Rev*., 2009, **38,** 2214–2230.

5 S. M. Bachilo, M. S. Strano, C. Kittrell, R. H. Hauge, R. E. Smalley, R. B. Weisman, *Science,* 2002, **298,** 2361–2366.

6 M. S. Strano, C. A. Dyke, M. L. Usrey, P. W. Barone, M. J. Allen, H. Shan, C. Kittrell, R. H. Hauge, J. M. Tour, R. E. Smalley, *Science,* 2003, **301,** 1519–1522.

7 R. Shvartzman-Cohen, E. Nativ-Roth, E. Baskaran, Y. Levi-Kalisman, I. Szleifer, R. Yerushalmi-Rozen, *J. Am. Chem. Soc.,* 2004, **126,** 14850–14857.

8 J. C. Grunlan, L. Liu, Y. S. Kim, *Nano Lett.,* 2006, **6,** 911–915.

9 M. Zheng, A. Jagota, E. D. Smeke, B. A. Diner, R. S. Mclean, S. R. Lustig, R. E. Richardson, N. G. Tassi, *Nat. Mater.,* 2003, **2,** 338–342.

10 A. Star, D. W. Steuerman, J. R. Heath, J. F. Stoddart, *Angew. Chem., Int. Ed.,* 2002, **41,** 2508–2512.

11 J. Lagerwall, G. Scalia, M. Haluska, U. Dettlaff-Weglikowska, S. Roth, F. Giesselmann, *Adv. Mater.,* 2007, **19,** 359–364.

12 H. Wang, G. T. Christopherson, Z. Y. Xu, L. Porcar, D. Ho, D. Fry, E. K. Hobbie, *Chem. Phys. Lett.,* 2005, **416,** 182–186.

13 M. J. Casavant, D. A. Walters, J. J. Schmidt, R. E. Smalley, *J. Appl. Phys.,* 2003, **93,** 2153–2156.

14 J. E. Fischer, W. Zhou, J. Vavro, M. C. Llaguno, C. Guthy, R. Haggenmueller, M. J. Casavant, D. E. Walters, R. E. Smalley, *J. Appl. Phys.* 2003, **93,** 2157–2163.

15 P. V. Kamat, K. G. Thomas, S. Barazzouk, G. Girishkumar, K. Vinodgopal, D. Meisel, *J. Am. Chem. Soc.,* 2004, **126,** 10757–10762.

16 S. Badaire, C. Zakri, M. Maugey, A. Derré, J. N. Barisci, G. Wallace, P. Poulin, *Adv. Mater.,* 2005, **17,** 1673–1676.

17 W. Song, I. A. Kinloch, A. H. Windle, *Science,* 2003, **302,** 1363–1363.

18 I. Dierking, G. Scalia, P. Morales, D. LeClere, *Adv. Mater.,* 2004, **16,** 865–869.

19 W. H. Song, A. H. Windle, *Macromolecules,* 2005, **38,** 6181–6188.

20 B. Vigolo, A. Pénicaud, C. Coulon, C. Sauder, R. Pailler, C. Journet, P. Bernier, P. Poulin, *Science,* 2000, **290,** 1331-1334.

21 F. Tardani, C. La Mesa, P. Poulin, M. Maugey, *J. Am. Chem. Soc.,* 2007, **129,** 9452-9457.

22 J. Loudet, P. Barois, P. Poulin, *Nature,* 2000, **407**, 611-613.

23 S. E. Moulton, M. Maugey, P. Poulin, G. G. Wallace, *J. Phys. Chem. C*, 2012, **116,** 9888-9894.

24 J. Lagerwall, G. Scalia, *J. Mater. Chem.*, 2008, **18**, 2890–2898.

25 J. Lagerwall, G. Scalia, M. Haluska, U. Dettlaff-Weglikowska, S. Roth, F. Giesselmann, *Adv. Mater.* 2007, **19**, 359–364.

26 G. Scalia, C. von Bühler, C. Hägele, S. Roth, F. Giesselmann, J. Lagerwall, *Soft Matter*, 2008, **4**, 570–576.

27 F. Tardani, C. Pucci and C. La Mesa, *Soft Matter,* 2014, **10**, 1024-1031.

28 F. Tardani, C. La Mesa, *J. Phys. Chem. C,* 2011, **115**, 9424 –9431.

29 F. Tardani, P. Strobbia, A. Scipioni, C. La Mesa, *RSC Adv.*, 2013, **3**, 25917-25923.

30 F. Tardani, L. Gentile, G. A. Ranieri, C. La Mesa, *J. Phys. Chem. C*, 2013, **117**, 8556 − 8562.

31 G. Scalia, J. P. Lagerwall, S. Schymura, M. Haluska, F. Giesselmann, S. Roth, *Phys. Stat. Sol. (b),* 2007, **244,** 4212–4217.

32 M. D. Lynch, D. L. Patrick, *Nano Lett.,* 2002, **2,** 1197–1201.

33 X. Xin, M. Pietraszkiewicz, O. Pietraszkiewicz, O. Chernyayeva, T. Kalwarczyk, E. Gorecka, D. Pociecha, H. Li, R. Hołyst, *Carbon*, 2012, **50,** 436–443.

34 X. Xin, H. Li, E. Kalwarczyk, A. Kelm, M. Fiałkowski, E. Gorecka, D. Pociecha, R. Hołyst, *Langmuir,* 2010, **26,** 8821–8828.

35 X. Xin, H. Li, S. A. Wieczorek, T. Szymborski, E. Kalwarczyk, N. Ziębacz, E. Gorecka, D. Pociecha, R. Holyst, *Langmuir,* 2010, **26,** 3562–3568.

36 M. S. Strano, C. A. Dyke, M. L Usrey, P. W. Barone, M. J. Allen, H. Shan, C. Kittrell, R. H. Hauge, J. M. Tour, R. E. Smalley, *Science,* **2003, 301,** 1519–1522.

37 V. C. Moore, M. S. Strano, E. H. Haroz, R. H.; Hauge, R. E. Smalley, *Nano Lett*., 2003, **3,** 1379–1382.

38 X. Xin, G. Xu, Y. Zhu, X. Shi, H. Gong, Z. Zhang, *J. Phys. Chem. C*., 2008, **112,** 16377–16384.

39 C. Richard, F. Balavoine, P. Schultz, T. W. Ebbesen, C. Mioskowski, *Science,* 2003, **300,** 775–778.

40 R. Holyst, K. Staniszewski, I. Demyanchuk, *J. Phys. Chem. B,* 2005, **109,** 4881–4886.

41 A. Zywocinski, A. Korda, J. Gosk, S. A. Wieczorek, A. Wilk, R. Holyst, *J. Am. Chem. Soc*., 2007, **129,** 13398–13399.

42 S. Makulska, E. Chudy, K. Urbaniak, S. A. Wieczorek, A. Zywocinski, R. Holyst, *J. Phys. Chem. B,* 2007, **111,** 7948–7953.

43 R. Holyst, A. Bielejewska, J. Szymański, A. Wilk, A. Patkowski, J. Gapiński, S. A. Wieczorek, Phys. Chem. Chem. Phys., 2009, **11,** 9025-9032.

44 G. Bouglet, C. Ligoure, A. M. Bellocq, E. Dufourc, G. Mosser. *Phy. Rev. E*, 1998, **57,** 834–842.

45 H. Li, J. Hao, *J. Phys. Chem. B,* 2008, **112,** 10497–10508.

46 L. S. Liyanage, D. J. Cott, A. Delabie, S. Van Elshocht, Z. Bao, H. P. Wong, *Nanotechnology,* 2013, **24,** 245703.

47 X. Chen, G. S. Lee, A. Zettle, C. R. Betozzi, *Angew. Chem., Int. Ed.,* 2004, **43,** 6111–6116.